

Article

Capacity Enhancement for Free Space Optics Transmission System Using Orbital Angular Momentum Optical Code Division Multiple Access in 5G and beyond Networks

Somia A. Abd El-Mottaleb ¹, Mehtab Singh ², Abdellah Chehri ^{3,*}, Hassan Yousif Ahmed ⁴, Medien Zeghid ^{4,5} and Akhtar Nawaz Khan ⁶

¹ Alexandria Higher Institute of Engineering and Technology, Alexandria 21311, Egypt

² Department of Electronics and Communication Engineering, University Institute of Engineering, Chandigarh University, Mohali 140413, Punjab, India

³ Department of Mathematics and Computer Science, Royal Military College of Canada, Kingston, ON K7K 7B4, Canada

⁴ Department of Electrical Engineering, College of Engineering in Wadi Alddawasir, Prince Sattam Bin Abdulaziz University, Wadi Alddawasir 11991, Saudi Arabia

⁵ Electronics and Micro-Electronics Laboratory (E. μ. E. L.), Faculty of Sciences, University of Monastir, Monastir 5000, Tunisia

⁶ Department of Electrical Engineering, Jaloza Campus, University of Engineering and Technology, Peshawar 25120, Pakistan

* Correspondence: chehri@rmc.ca



Citation: El-Mottaleb, S.A.A.; Singh, M.; Chehri, A.; Ahmed, H.Y.; Zeghid, M.; Khan, A.N. Capacity Enhancement for Free Space Optics Transmission System Using Orbital Angular Momentum Optical Code Division Multiple Access in 5G and beyond Networks. *Energies* **2022**, *15*, 7100. <https://doi.org/10.3390/en15197100>

Academic Editor: Alberto Geri

Received: 25 August 2022

Accepted: 20 September 2022

Published: 27 September 2022

Publisher's Note: MDPI stays neutral with regard to jurisdictional claims in published maps and institutional affiliations.



Copyright: © 2022 by the authors. Licensee MDPI, Basel, Switzerland. This article is an open access article distributed under the terms and conditions of the Creative Commons Attribution (CC BY) license (<https://creativecommons.org/licenses/by/4.0/>).

Abstract: This paper introduces a novel free space optics (FSO) communication system for future-generation high-speed networks. The proposed system integrates orbital angular momentum (OAM) modes with an optical code division multiple access (OCDMA) technique. Two OAM beams are used ($LG_{0,0}$ and $LG_{0,10}$), each of which is used for transmitting three independent channels. Each channel is assigned by fixed right shift (FRS) codes and carries 10 Gbps of information data. The performance of the proposed model is evaluated under different foggy and dust storm conditions. Furthermore, the performance of two cities with different geographical locations, Alexandria city in Egypt and Srinagar city in India, is investigated to demonstrate its ability to be implemented in future generations. Bit error rate (BER), eye diagrams, received optical power (ROP), and channel capacity are used for studying the performance of the proposed system. The observed simulation results show successful transmission of 60 Gbps overall capacity with the longest propagation FSO range for Alexandria city, which is 1400 m. Because dust storms have a large attenuation when compared to different foggy conditions, the proposed model had the shortest propagation range of 315 m under low dust (LD), 105 m under moderate dust (MD), and 40 m under heavy dust (HD). Furthermore, the cloudy weather conditions that affect Srinagar city, which is considered a hilly area, make our suggested model achieve 1000 m.

Keywords: space division multiplexing; orbital angular momentum; free space optics; optical code division multiple access; fixed right shift; bit error rate

1. Introduction

The rapid evolution of today's telecommunications networks is driven by users' need to stay connected anytime, anywhere. From the intelligent telephone network to today's high-speed wide area networks, the rapid evolution of communication networks has been accompanied by the people's social needs, from the growing demand for users to new applications.

Even with the arrival of the fifth-generation networks (5G), an excessive increase in the number of subscribers using smartphones and social networking applications makes the demand for high-speed data rates rise exponentially, which leads to a telecommunication

bottleneck. As a result, the need to investigate new alternatives to the existing radio frequency (RF) infrastructure has become urgent.

Communication research has already shifted from 5G to the beyond-5G (or sixth-generation, 6G) networks, labeled the B5G/6G era. The RF regime cannot afford the evolution of data-hungry applications requiring high-speed data transmission and receiving [1–3]. Instead, the optical domain, with frequencies a thousand times higher, is an envisaged solution to improve the network's throughput. Therefore, the upcoming networks are expected to use higher-frequency bands than are currently in use.

Free space optics (FSO) is a communication system that uses free space as a channel for sending signals carrying information [4]. It is technologically very close to optical fiber communication (OFC) in terms of optical modulated signal transmission. It supports high data transmission, unlicensed spectrum, as it uses light, and a high level of secure transmission [5,6]. Additionally, it has the good advantage that it can be implemented in places where the geographical locations make the installation of optical fiber difficult [7].

Figure 1 depicts the various areas where FSO can be implemented, such as hospitals, submarines, business buildings, and agriculture farms.

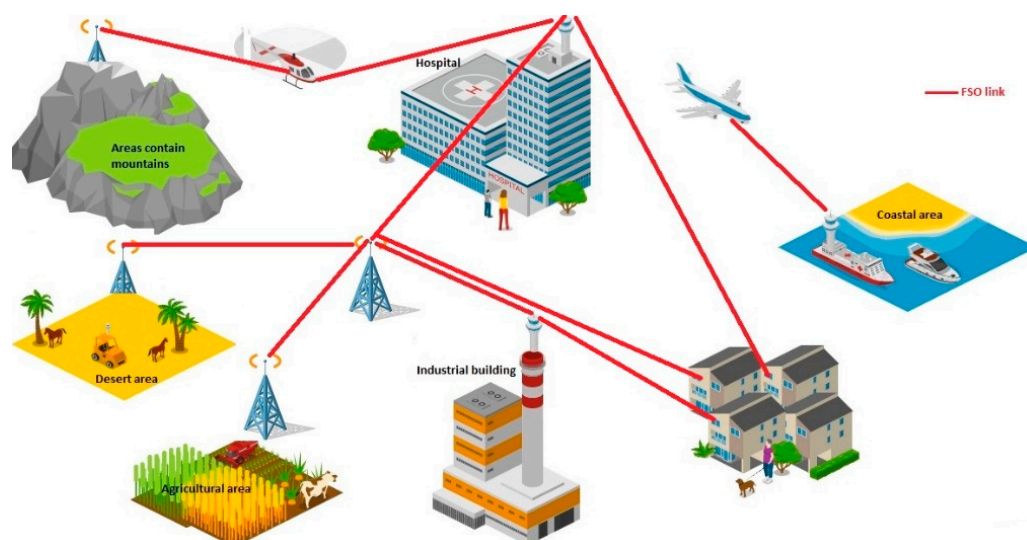


Figure 1. Different areas where FSO link can be applied for 5G and beyond network.

As clear from Figure 1, a high-speed FSO link can help patients living in remote areas to be supervised by doctors in central hospitals. In addition, people who live in the regions that contain mountains can use the FSO link to transmit and receive their information, as in these areas, the installation of cables will be complicated. Additionally, in agricultural fields, people who live in smart households can monitor their work on their farms using the FSO link.

Although FSO communication has several advantages, other external challenges such as weather conditions affect its performance. For example, the different weather conditions cause attenuation to the information signal, leading to a higher bit error rate value (BER) [8]. According to climate condition, the value of attenuation differs, as for clear weather, its value is less than 1 dB/km, while for heavy dust (HD) storms, its value becomes hundreds of dB/km [9].

Nowadays, researchers use different multiplexing techniques in FSO communication in order to increase the capacity and allow multiple users to transmit their data over the FSO channel. Some of these techniques are wavelength division multiplexing [10,11], orthogonal frequency division multiplexing [12,13], and polarization division multiplexing [14].

Recently, optical code division multiple access (OCDMA) has gained attention in FSO communication. It is based on the presence of light, as a binary “1” indicates the presence of light and wavelength, whereas a binary “0” indicates the absence of light. Multiple users

in OCDMA can use the same channel at the same time while transmitting data with a high level of security [6,7].

In [12], the authors proposed an FSO system by integrating OFDM with mode division multiplexing (MDM) using a 4-QAM scheme. The results showed a successful transmission capacity of 40 Gbps under the effect of different dust storms. The performance of hybrid PDM with SAC-OCDMA was also evaluated in [14], and the obtained results showed successful transmission of 10 channels with 50 Gbps of information capacity.

Recently, space division multiplexing (SDM) has been introduced into FSO communication that is based on the spatial distribution of electromagnetic (EM) waves. Mode division multiplexing (MDM) is one type of SDM in which multiple independent information data can be transmitted using two or more overlapping orthogonal modes, leading to transmission capacity enhancement [15].

Orbital angular momentum (OAM) modes are considered suitable for carrying the information data in FSO communication systems, among the other orthogonal modes employed. Its orthogonal nature makes it easier for multiplexing or de-multiplexing with low inter-channel crosstalk [16]. Additionally, the intensity of OAM beams has a donut ring pattern, while as these beams propagate, their phase rotates in a helical pattern. The generation of the OAM beams through the diffractive optics can be achieved by three methods. These methods are diffractive optical elements, computed-generated holograms, and spiral phase plates [17]. As for detecting the OAM beams, researchers proposed several methods to detect them. The far-field diffraction patterns of triangular apertures, wedged optical flats, twisted phases, Fresnel bi prisms, and tilted converging cylindrical or spherical lenses are used in these methods [18].

Furthermore, to increase the overall FSO system capacity, researchers integrate other multiplexing techniques with OAM such as QPSK [19], WDM and PDM [20], and OFDM [21].

The performance of OFDM in FSO using 16-quadrature amplitude modulation (QAM) under fog conditions was studied for two Indian cities in [22]. The conducted results show improvements in the system performance. Still, the authors did not consider the separate compensation mechanism to solve the effects of weather conditions of the channel on the received signal. This is clear from the constellation plots of the received signal that have unwanted phase shifts.

In [23], the authors used spectrum slicing with WDM in the FSO system and studied the system's performance for the weather conditions of southern India. They used 16 channels; each carried 1.56 Gbps information. In [24], the performance of WDM in the FSO system was studied for desert areas. The proposed model achieved low data rates ranging from 0.3 Gbps to 0.7 Gbps. However, the authors used laser power of 50 dBm, which is not safe for human eyes [25].

The performance of an FSO system that uses QAM and quadrature phase shift keying (QPSK) modulation was studied by authors in [26]. As multiple symbols are transmitted simultaneously in these modulation techniques, information may be lost due to inter-symbol interference.

In [27], the authors studied the performance of four independent channels transporting 10 Gbps of data transmitted on four distinct OAM beams in an FSO system under various weather conditions. The obtained results revealed successful transmission of 40 Gbps. QPSK modulated signals transported using two different OAM beams were demonstrated experimentally in [28]. The authors concluded a successful transmission of 80 Gbps unmanned aerial vehicle (UAV) to ground terminal FSO.

This paper proposes a novel FSO communication system that integrates two OAM beams with spectral amplitude coding optical code division multiplexing (SAC-OCDMA) using fixed right shift code (FRS) for capacity improvement and secure transmission of data.

The Main Contributions of This Paper

- Enhance capacity through proposing a new FSO system based on integrating OAM with OCDMA using FRS code.

- Assign FRS code with OCDMA and use single photodiode detection (SPD) technique.
- Study the performance of the proposed FSO model under different foggy conditions.
- As there is lack of study of the effect of dust storms, we study the performance of our model under different dust storms.
- Use two different cities having different geographical locations and different weather conditions that are Alexandria city in Egypt and Srinagar city in India and study the performance of the suggested model under their weather conditions.

The remainder of the paper is structured as follows. Section 2 illustrates the code property and construction of FRS code followed by the proposed model description in Section 3. Section 4 shows the mathematical analysis in terms of BER of our suggested model. Finally, obtained simulation results are discussed in Section 5, followed by main conclusions and suggested applications for our FSO model are drawn in Section 6.

2. Fixed Right Shift Code (Related Works)

This code is characterized by L , P , λ_{cross} , and N_u , that represent, respectively, code length, code weight, cross-correlation between any two code sequence, and number of simultaneous users.

The relation between L and N_u can be given as [29]:

$$L = N_u (P - 2) + P \quad (1)$$

The minimum value for P is 3 and the FRS code must obtain the condition of $(P - 2)$ fixed right shift of unity. As its construction depends on selecting the values of P and N_u , whether even or odd, that makes the FRS code construction vary. The basic matrix $N_u \times L$ of the code contains first nonzero ($1^{st}NZ$) elements and last nonzero elements (LNZ) and can be expressed as [29]:

$$B_M = \begin{bmatrix} 1^{st}NZ_1 & LNZ_1 & 0 & \dots & \dots & \dots & 0 \\ 0 & 1^{st}NZ_2 & LNZ_2 & 0 & \dots & \dots & 0 \\ 0 & 0 & 1^{st}NZ_3 & LNZ_3 & 0 & \dots & \vdots \\ \vdots & \vdots & \vdots & \ddots & \ddots & \ddots & \vdots \\ 0 & 0 & 0 & 0 & 0 & 1^{st}NZ_U & LNZ_U \end{bmatrix} \quad (2)$$

Thus, it is important to know the position of both $1^{st}NZ$ and LNZ elements in the matrix. Let W be the number of rows that has values ranging from 1 to N_u , so the $1^{st}NZ$ can be placed at $(W, 1 + (W - 1)(P - 2))$. As for LNZ , it can be placed at $(W, 1 + (W - 1)(P - 2) + 2P - 3)$. As for the other elements of the matrix, they can be filled as follows: fill $(P - 2)$ with "1 s" after $1^{st}NZ$ and $(P - 2)$ with "0 s" before LNZ .

As an example that is used in this study, we take $P = 3$, $N_u = 3$, so the value of L according to Equation (1) will be 6. Thus, the matrix will be 3×6 . Therefore, we have three rows and each row has $1^{st}NZ$ and LNZ elements. As for the first row, $W = 1$, the place of $1^{st}NZ$ and LNZ , respectively, will be at (1,1) and (1,4), while for $W = 2$, $1^{st}NZ$ is located at (2,2) while LNZ is located at (2,5). The last row has the position of $1^{st}NZ$ at (3,3) and the position of LNZ at (3,6). As for the other elements of the matrix, we fill "1 s" $(P - 2) = 3 - 2 = 1$ after $1^{st}NZ$ and "0 s" with "0 s" before LNZ . Then the 36 FRS code matrix will be expressed as [29]:

$$M_{3 \times 6} = \begin{bmatrix} 1 & 1 & 0 & 1 & 0 & 0 \\ 0 & 1 & 1 & 0 & 1 & 0 \\ 0 & 0 & 1 & 1 & 0 & 1 \end{bmatrix} \quad (3)$$

3. OAM Beams and Laguerre–Gaussian (LG) Modal Analysis

Light waves can carry OAM beams, which are characterized by the helical phase front of a light beam that is represented by $e^{im\varnothing}$, where m and \varnothing , respectively, represent the number of 2π phase shifts in the phase profile of beam and the azimuthal angle [30].

Figure 2 shows the donut shape of the OAM beam (wave front, intensity, and phase) with different values of m .

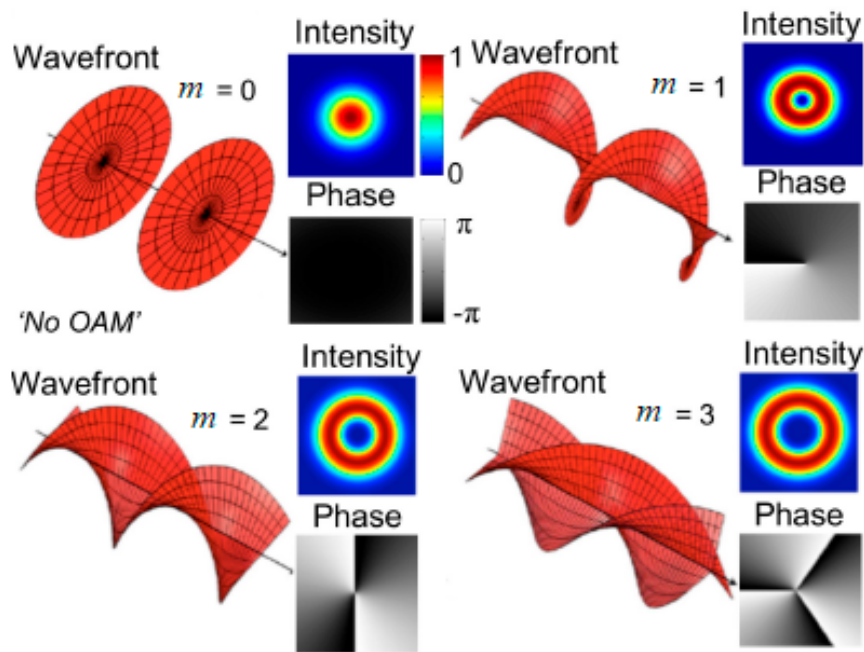


Figure 2. Donut shape of OAM beam with $m = 0, 1, 2, 3$ [29].

OAM beams can have an infinite number of states, where m can be any integral value. OAM beams are orthogonal while propagating coaxially with each other. As an example, consider two different OAM beams with m_1 and m_2 , respectively [31]:

$$u_1(\rho, \varnothing, z) = A_1(\rho, z)e^{im_1\varnothing} \tag{4}$$

$$u_2(\rho, \varnothing, z) = A_2(\rho, z)e^{im_2\varnothing} \tag{5}$$

where ρ refers to radial and z is the direction of propagation and (ρ, \varnothing, z) is the cylindrical coordinate. The orthogonality between two different OAM beams can be given as [32]:

$$\int_0^{2\pi} u_1(\rho, \varnothing, z)u_2^*(\rho, \varnothing, z)d\varnothing = \begin{cases} 0 & \text{if } m_1 \neq m_2 \\ A_1A_2^* & \text{if } m_1 = m_2 \end{cases} \tag{6}$$

As an OAM beam refers to any helically phased light beam, regardless of its radial distribution, the Laguerre–Gaussian (LG) modes are used for a complete two-dimensional (2D) modal analysis. The LG modes have both m for azimuthal distribution and p for radial distribution [33,34].

The mathematical description of the electric field of the LG, $\psi(\rho, \phi, z; m, p)$, in cylindrical coordinate is given by [30,35]:

$$\begin{aligned} \psi(\rho, \phi, z; m, p) = & \sqrt{\frac{2p!}{\pi(p+|m|)!}} \frac{1}{\omega(z)} \left[\frac{r\sqrt{2}}{\omega(z)} \right]^{|m|} L_{p,m} \left[\frac{2r^2}{\omega^2(z)} \right] \\ & \times \exp \left[\frac{-r^2}{\omega^2(z)} \right] \exp \left[\frac{-icr^2z}{2(z^2+z_R^2)} \right] \\ & \times \exp \left[i(2p + |m| + 1)\tan^{-1} \frac{z}{z_R} \right] \exp(-im\varnothing) \end{aligned} \tag{7}$$

where ρ , ϕ , z , $\omega(z)$, and z_R represent radial coordinate, angular coordinate, direction of propagation along z -axis, waist size of beam at z -distance, and Rayleigh range, respectively. $L_{p,m}$ is LG polynomial (p and m are modal indices in ρ direction and ϕ direction, respectively) and c is the optical wave number that is equal to $2\pi/\lambda$.

For a given $\omega(z)$ and z , the orthogonality between LG beams that have different values of m and/or p can be represented as [33,34,36]:

$$\int_0^{\infty} \int_0^{2\pi} \psi(\rho, \phi, z; m, p) \psi^*(\rho, \phi, z; m, p) \rho d\phi d\rho = \begin{cases} 0 & \text{if } m_1 \neq m_2 \text{ or } p_1 \neq p_2 \\ 1 & \text{if } m_1 = m_2 \text{ and } p_1 = p_2 \end{cases} \quad (8)$$

OAM can be utilized in FSO communication systems and enhance the capacity of the system through mode division multiplexing (MDM), which is a subset of SDM [37,38].

Each OAM beam can carry the same p value and different values of m in LG modes or the same m value and different p values. In this work, we considered the same m value that is 0 and different p values that are 0 and 10. Theoretically infinite modes are possible, but due to the limitations of OAM modes multiplexing and de-multiplexing techniques and higher inter-modal crosstalk due to a large number of modes, we used only two modes in this study.

4. Proposed System Design

The architecture of the proposed OAM/OCDMA-FSO system is given in this section. It consists of transmitter, channel, and receiver.

4.1. OAM/OCDMA-FSO Transmitter

As shown in Figure 3, the transmitter of our system consists of three parts: optical source, information, and SAC-OCDMA encoder. The optical source is the spatial laser (SL), which generates two distinct OAM beams ($LG_{0,0}$, $LG_{0,10}$).

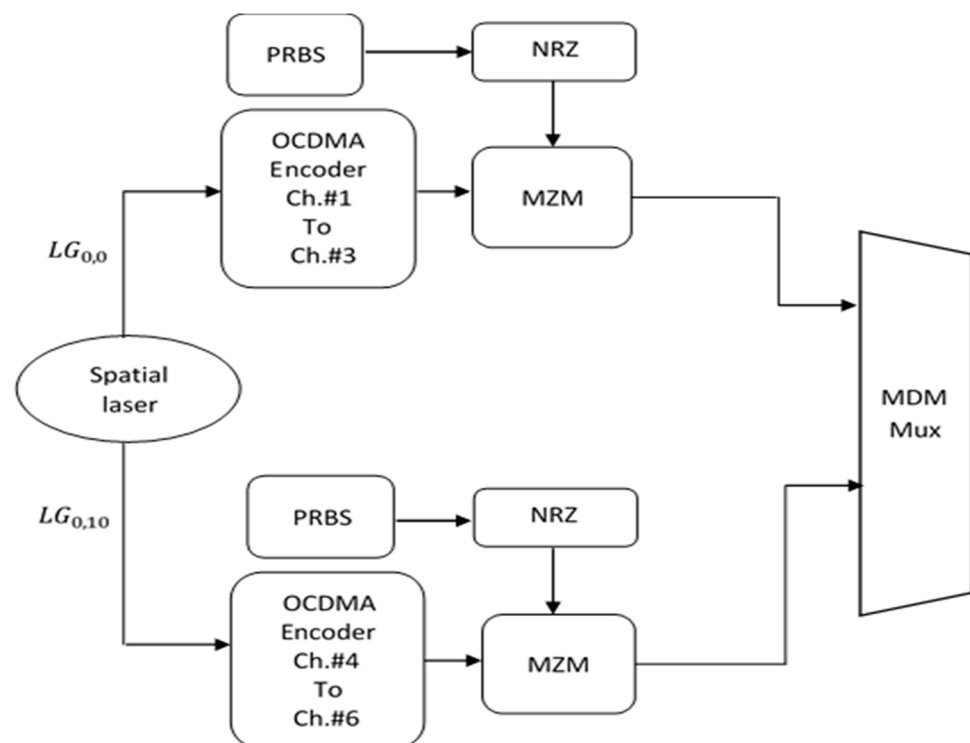


Figure 3. Block diagram demonstrating the transmitter of the OAM/OCDMA-FSO system (MZM: Mach–Zehnder modulator; PRBS: pseudorandom bit sequence).

As for the information bits, a pseudorandom bit sequence (PRBS) generator is used for generating 10 Gbps for each channel, while a non-return to zero (NRZ) modulator is used to encode the binary data. In the FRS encoder, specific wavelengths (optical carriers) that are generated from the optical source are combined according to the assigned FRS code using an optical coupler according to the assigned code.

The wavelengths that are assigned to the channels used in the proposed model are given in Table 1.

Table 1. Wavelengths assigned to the channels of the FRS encoder.

Wavelength (nm)		1550	1550.8	1551.6	1552.4	1553.2	1554
$LG_{0,0}$	Channel #1	1	1	0	1	0	0
	Channel #2	0	1	1	0	1	0
	Channel #3	0	0	1	1	0	1
$LG_{0,10}$	Channel #4	1	1	0	1	0	0
	Channel #5	0	1	1	0	1	0
	Channel #6	0	0	1	1	0	1

The Mach–Zehnder modulator (MZM) is used to modulate the electrical signal that carries 10 Gbps optical signal modulated over the two distinct OAM beams ($LG_{0,0}$, $LG_{0,10}$).

The resulting modulated signal from the MZM is further combined with the other signals from the other channels before transmitting to the free-space channel.

4.2. FSO Channel

The FSO channel is used in our proposed model. Various weather conditions will have impact on the channel due to the attenuation caused by them. Therefore, in this study, we focus on the effect of different fog levels and different dust storms on the proposed OAM/OCDMA-FSO system performance during transmission between the transmitter and receiver.

Furthermore, the effect of weather conditions of two cities, one in Egypt that is Alexandria and the other in India that is Srinagar, are also investigated in this study so as to show the proof of concept of our proposed system in a real environment.

4.2.1. Fog Weather Conditions

Fog is an atmospheric phenomenon that is well known as a cloud of either water particles or smoke particles that reduce the visibility and cause attenuation which degrades the received signal. According to the amount of smoke particles and quantity of water particles suspended in the atmosphere, fog varies from light fog (LF) to moderated fog (MF) to heavy fog (HF). These diverse fog levels cause different attenuation.

The attenuation of fog increases as the quantity of microscopic water droplets suspended in the atmosphere increases, and that causes fog to become heavier. Thus, different fog levels LF, MF, and HF have different attenuations. Fog attenuation, f_a , in dB/km that depends on visibility range, R , in km, can be expressed as [25]:

$$f_a = \frac{3.912}{R} \left(\frac{\lambda}{550\text{nm}} \right)^{-b} \quad (9)$$

where λ is the operating wavelength in (nm) and b is the size distribution of the scattering particles that can be calculated according to Kim's model [30].

Different fog levels with their attenuation are shown in Table 2 [39]:

$$b = \begin{cases} 1.6 & R > 50 \\ 1.3 & 6 < R < 50 \\ 0.16R + 0.34 & 1 < R < 6 \\ R - 0.5 & 0.5 < R < 1 \\ 0 & R < 0.5 \end{cases} \quad (10)$$

Table 2. Fog level with attenuation [39].

Fog Level	Attenuation (dB/km)
LF	9
MF	16
HF	22

4.2.2. Dust Storm Weather Conditions

Dust storms, caused by strong winds that pull the dust from the ground up into the air, have effects on the FSO link. The World Meteorological Organization (WMO) classifies dust storms according to their strength into four categories: dust haze (DH), light dust (LD), medium dust (MD), and heavy dust (HD) [39]. Dust storms also cause attenuation during the transmission between the transmitter and receiver that degrades the received signal. This attenuation, D_a , in dB/km, that depends on R can be expressed as [27]:

$$D_a = 52 \times R^{-1.05} \quad (11)$$

Table 3 shows the visibility and the attenuation corresponding to different levels of dust storms [9,24].

Table 3. Dust storm level with visibility and attenuation [9,24].

Dust Level	LD	MD	HD
Visibility (km)	1–10	0.2–1	<0.2
Attenuation (dB/km)	25.11	107.66	297.38

4.2.3. Weather Conditions of Alexandria and Srinagar Cities

In this study, we consider the effect of weather on two different cities in two different continents that are Alexandria, located in Egypt, Africa, and Srinagar, located in India, Asia.

According to www.weatherspark.com (accessed on 1 May 2022), the weather of Alexandria city in summer is warm, arid, and clear, while in winter, it is cool, windy, and mostly clear. As for Srinagar city, the weather in summer is warm and clear, while in winter, it is very cold and partly cloudy.

As for visibilities, the meteorological data for daily visibility for Alexandria city are obtained from www.worldweatheronline.com (accessed on 1 May 2022) for the years 2014 to 2018, while the daily visibility for Srinagar is obtained from the Indian Meteorological Department for the years 2014 to 2018 [40].

Alexandria city has a recorded average R of 9.8 km, while for Srinagar city, the recorded average R is 2.9 km. According to Equations (9) and (10), the attenuation of Alexandria and Srinagar cities are calculated and tabulated in Table 4.

Table 4. Visibilities and attenuations of Alexandria and Srinagar cities.

City	Alexandria	Srinagar
Visibility (km)	9.8	2.9
Attenuation (dB/km)	0.1	2.48

4.3. OAM/OCDMA-FSO Receiver

Figure 4 illustrates the block diagram of the receiver of the OAM/OCDMA-FSO system. The MDM demultiplexer is used at the receiver first to separate the two OAM beams; then, the received signal undergoes the decoding process that has the SPD detection to detect the desired channel.

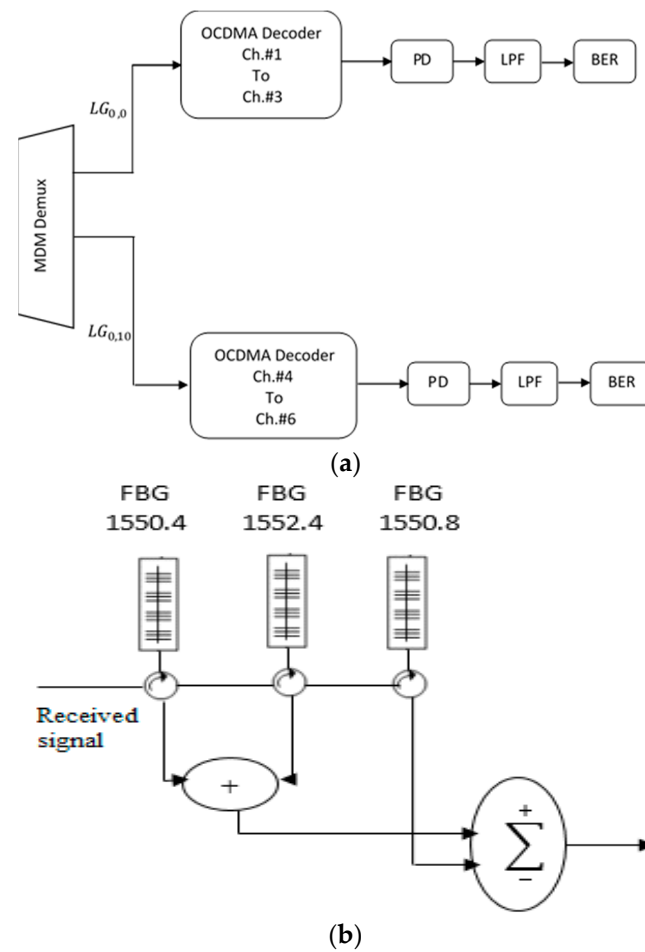


Figure 4. Block diagram demonstrating the receiver of the OAM/OCDMA-FSO system. (a) Receiver structure and (b) example of OCDMA decoder of user 1.

In SPD detection, the received signal first passes through the decoder then the subtractive decoder (S-dec). The decoder has the same spectral profile as that of the encoder.

As an example, let us consider that channel #1 is the required channel, so the decoder will have these wavelengths in nm (1550, 1550.8, and 1552.4), while for s-dec, it contains wavelength 1550.8 nm, which is the interference with channel #2. Then the s-dec is subtracted from the decoder.

The resulting signal now carries the information of the desired channel #1 and then enters the PIN photodiode detector (PD) to make the electric/optical conversion. Finally, the output received signal is transferred to a low-pass Bessel filter.

5. Mathematical Analysis of Proposed OAM/OCDMA-FSO Model

The FRS code property when SPD detection is used is

$$\sum_{j=1}^L H_x(j) \cdot H_y(j) - \sum_{j=1}^L (H_x(j) \cdot H_y(j) \cdot H_x(j)) = \begin{cases} P - 1, & \text{for } x = y \\ 0, & \text{for } x \neq y \end{cases} \quad (12)$$

where $H_x(j)$ and $H_y(j)$ represent the j th element of the X and Y code sequence.

The power spectral density (PSD), $P(v)$, at PIN PD is [41]:

$$P(v) = \frac{R_p}{\Delta v} \sum_{i=1}^U d_U \left(\sum_{j=1}^L H_x(j) \cdot H_y(j) - \sum_{j=1}^L (H_x(j) \cdot H_y(j) \cdot H_x(j)) \right) \left\{ u \left[\frac{\Delta v}{L} \right] \right\} \quad (13)$$

where Δv and $u\left[\frac{\Delta v}{L}\right]$, respectively, represents optical bandwidth and unit step function.

The current received at PIN PD, I_U , is expressed by [41]:

$$I_U = \mathcal{R} \int_0^\infty P(v)dv = \mathcal{R} \left(\frac{R_p(P-1)}{L} \right) \quad (14)$$

where \mathcal{R} is PIN PD responsivity, and R_p is the received power, and, in the case of FSO link, is expressed as [42]:

$$R_p = T_p \left(\frac{D_{RX}}{D_{TX} + \theta S} \right)^2 10^{\frac{-\beta S}{10}} \quad (15)$$

where R_p and T_p , respectively, are transmitted and received power. D_{TX} is transmitted diameter while D_{RX} is the received diameter. S denotes propagation range, θ , indicates divergence angle of laser beam, and β is the atmospheric attenuation.

The shot noise power, P_{Sh} , is [43]:

$$P_{Sh} = 2 e B_{electric}(I_U) = \mathcal{R} \left(\frac{R_p(P-1)}{L} \right) \quad (16)$$

where e is electron charge and $B_{electric}$ is electrical bandwidth.

The PIIN noise power, P_{PN} , is [44]:

$$P_{PN} = \mathcal{R} \int_0^\infty (P(v))^2 dv = \frac{\mathcal{R}^2 B_{electric}^2 R_p^2 N_u P^2}{L^2 \Delta v} (P-1) \quad (17)$$

Thermal noise can be expressed as [45]:

$$P_{Th} = \frac{4k_B T B_e}{R_L} \quad (18)$$

where k_B is Boltzmann constant, and R_L and T are load resistance of receiver and absolute temperature of receiver noise, respectively.

The signal-to-noise ratio, SNR, is [7]:

$$\text{SNR} = \frac{(I_U)^2}{P_{Sh} + P_{PN} + P_{Th}} \quad (19)$$

The BER can be expressed as [25]:

$$\text{BER} = 0.5 \text{erfc} \left(\sqrt{\frac{\text{SNR}}{8}} \right) \quad (20)$$

where erfc is a complementary error function.

Table 5 shows the parameters used in the proposed OAM/OCDMA-FSO system that are evaluated and simulated using Optisystem software version 18 [12,46,47].

Table 5. Parameters used in the simulation [12,46,47].

Parameter	Value
Power of spatial laser	15 dBm
Laser wavelength	1550 nm
Laser linewidth	10 MHz
Spatial modes	$LG_{0,0}$, $LG_{0,10}$
Bit rate/channel	10 Gbps
Electrical bandwidth	$0.75 \times \text{bit rate Hz}$

Table 5. Cont.

Parameter	Value
Sequence length	1024
Samples	32
Transmitter aperture diameter (D_{TX})	10 cm
Receiver aperture diameter (D_{RX})	20 cm
Beam divergence angle (θ)	0.25 mrad
Photodiode responsivity (\mathcal{R})	1 A/W
Thermal noise power density	10^{-22} W/Hz

6. Results and Discussion

This part elucidates the simulation results of the proposed OAM/OCDMA-FSO system [48–51]. The results are divided into four sections, as follows.

6.1. Intensity Profile of Two OAM Beams

The spatial intensity patterns for OAM beams that are used in this study are given in Figure 5.

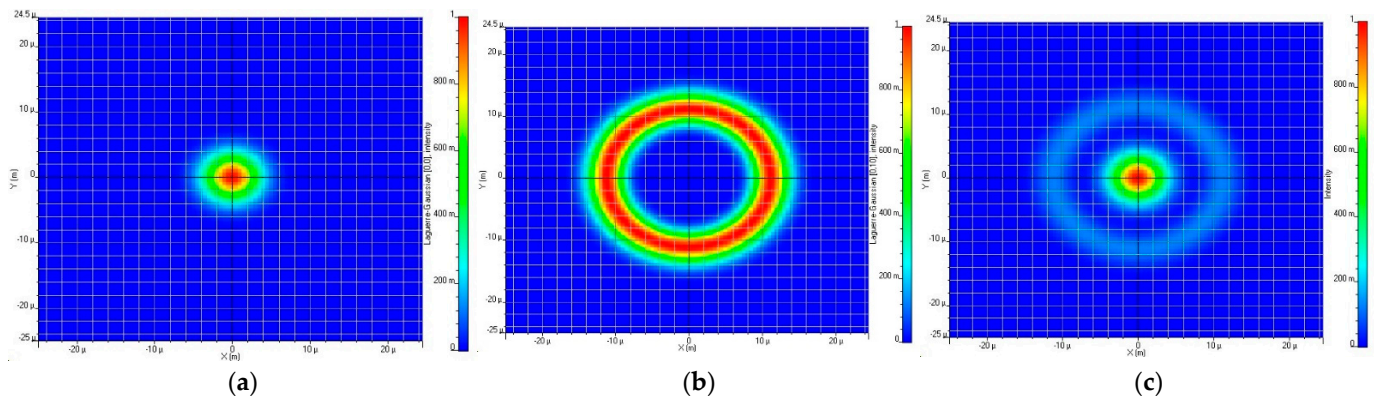


Figure 5. Spatial intensity profiles: (a) $LG_{0,0}$; (b) $LG_{0,10}$; (c) multiplexed mode.

6.2. Effect of Fog Conditions on OAM/OCDMA-FSO System

The performance of our proposed system is evaluated under different fog conditions: LF, MF, and HF. Figure 6a–c show the $\log(\text{BER})$ values against the propagation range. When the water droplets suspended in the air increase, the level of fog increases and the attenuation increases, resulting in shortening of the FSO link.

It is noticed that all channels under LF can propagate longer distances than under MF and HF. Channels 1 and 4 that propagate using $LG_{0,0}$ and $LG_{0,10}$, respectively, give the best $\log(\text{BER})$ values, which are -25.41 and -25.08 under LF at 600 m, -25.22 and -25.5 under MF at 425 m, and -24.9 and -24.75 under HF at 340 m. The lowest performance is for channel #3 that propagates using $LG_{0,0}$ and channel #6 that propagates using $LG_{0,10}$ OAM beam but is still accepted as it is less than the threshold value of -2.56 .

Figure 7 displays the eye diagrams for the six channels under LF at 600 m FSO range. All channels have wide eye openings, and this reveals good receiving for the transmitted information.

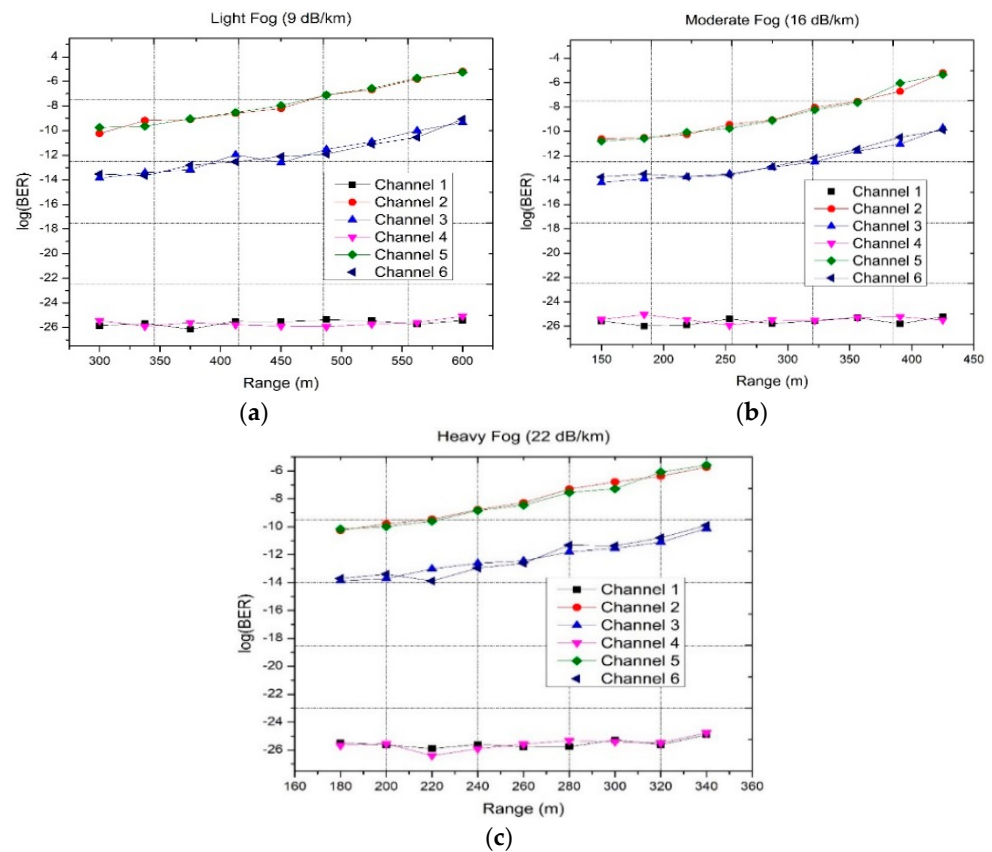


Figure 6. $\log(\text{BER})$ against FSO link for OAM/OCDMA-FSO system under (a) LF, (b) MF, and (c) HF.

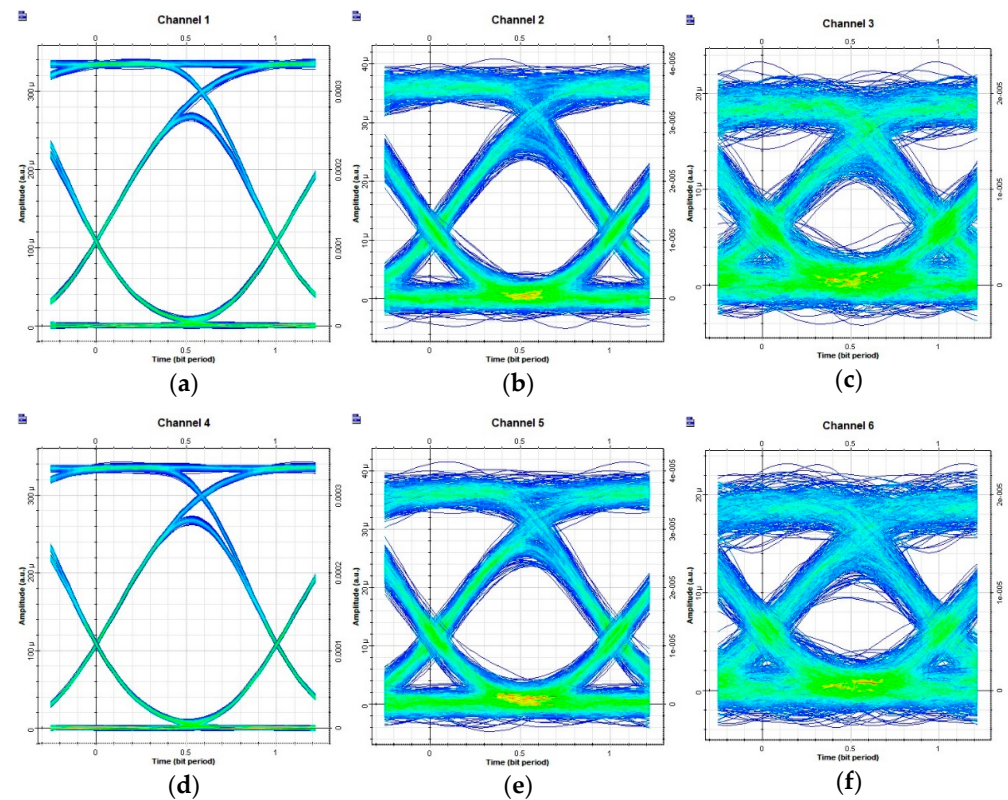


Figure 7. Eye diagrams for (a) channel #1, (b) channel #2, (c) channel #3, (d) channel #4, (e) channel #5, and (f) channel #6 under LF at 600 m FSO range.

Table 6 tabulates the $\log(\text{BER})$ values at maximum achieved propagation range for our proposed model under different fog conditions (600 m under LF, 425 m under MF, and 340 m under HF).

Table 6. $\log(\text{BER})$ values under different fog conditions for OAM/OCDMA-FSO system for six channels.

Channels	OAM Beams	$\log(\text{BER})$		
		LF (600 m)	MF (425 m)	HF (340 m)
Channel #1	$LG_{0,0}$	−25.41	−25.22	−24.9
Channel #2		−5.18	−5.19	−5.73
Channel #3		−9.34	−9.72	−10.12
Channel #4	$LG_{0,10}$	−25.08	−25.5	−24.75
Channel #5		−5.25	−5.34	−5.59
Channel #6		−9.06	−9.89	−9.9

6.3. Effect of Dust Conditions on OAM/OCDMA-FSO System

The performance of our proposed system is evaluated under various dust conditions, LD, MD, and HD, in this subsection. As dust storms pull the dust from the ground up into the air, this leads to smaller visibility range and higher attenuation value than that caused by fog conditions.

This attenuation causes signal degradation during the transmission of information. The values of BER are plotted versus different FSO links under different dust conditions for our proposed model in Figure 8a–c.

Comparing Figure 8 with Figure 9, one can notice that the maximum achievable FSO range for our proposed system is shorter in the case of various dust storms than in the case of fog conditions.

The maximum propagation ranges for all six channels under LD, MD, and HD are 315 m, 105 m, and 40 m, respectively, with BER less than 10^{-5} .

Table 7 summarizes the $\log(\text{BER})$ values at maximum achieved propagation range for our proposed model under different dust conditions (315 m under LD, 105 m under MD, and 40 m under HD).

Table 7. $\log(\text{BER})$ values under different dust conditions for OAM/OCDMA-FSO system for six channels.

Channels	OAM Beams	$\log(\text{BER})$		
		LD (315 m)	MD (105 m)	HD (40 m)
Channel #1	$LG_{0,0}$	−25.49	−25.18	−24.92
Channel #2		−5.59	−5.01	−5.83
Channel #3		−9.83	−9.5	−10.23
Channel #4	$LG_{0,10}$	−25.15	−25.47	−24.77
Channel #5		−5.67	−5.15	−5.69
Channel #6		−9.53	−9.66	−10.01

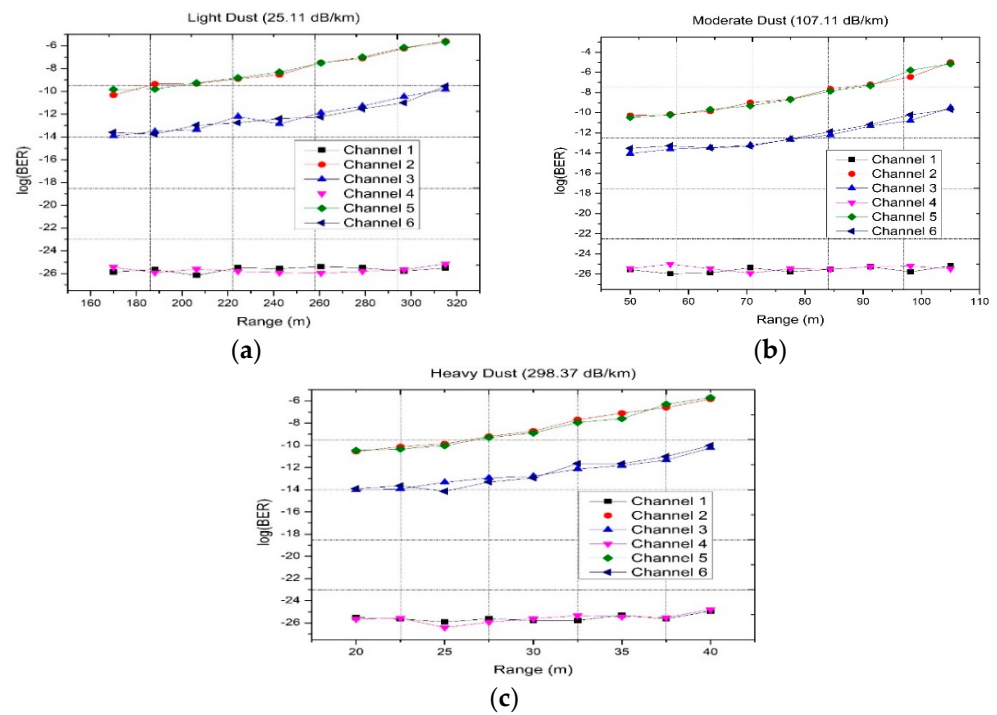


Figure 8. Log(BER) against FSO link for OAM/OCDMA-FSO system under (a) LD, (b) MD, and (c) HD.

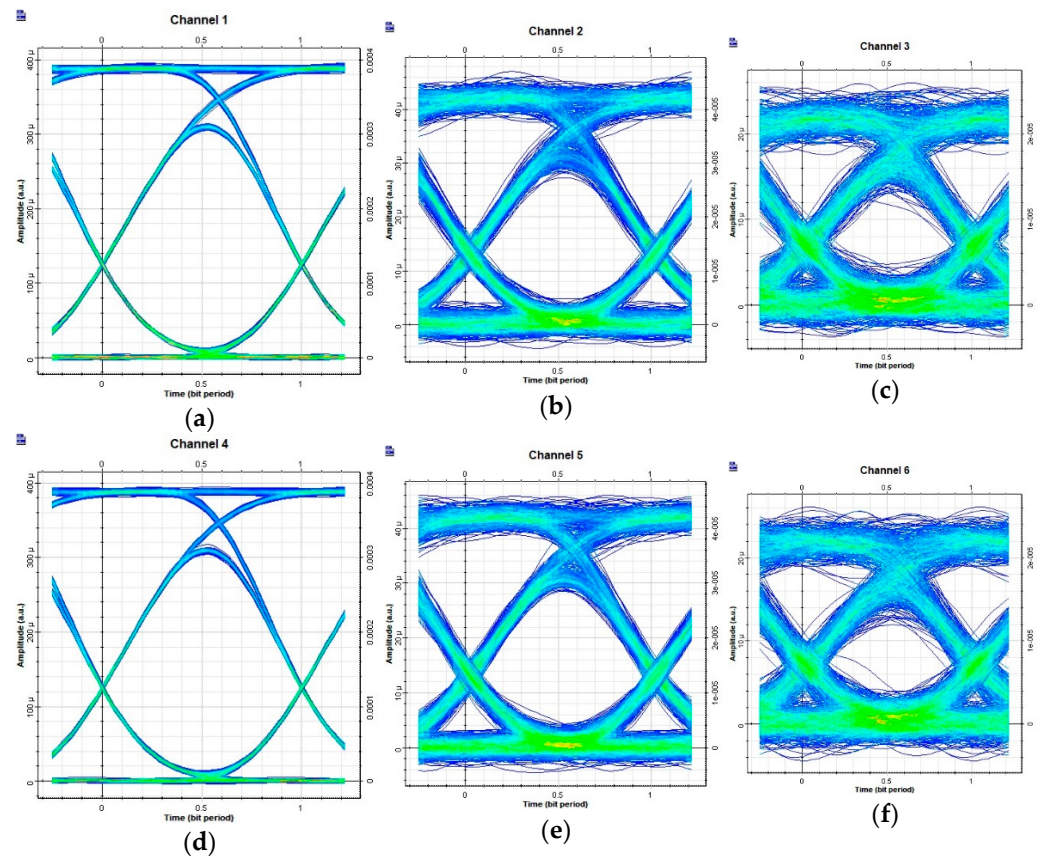


Figure 9. Eye diagrams for (a) channel #1, (b) channel #2, (c) channel #3, (d) channel #4, (e) channel #5, and (f) channel #6 under HD at 40 m FSO range.

6.4. Application of Using Proposed System in Alexandria City and Srinagar City

As Alexandria city has clearer weather than Srinagar city, it can achieve longer transmission distance in FSO. Figures 10 and 11 show the maximum propagation range that all channels achieved in Alexandria city and Srinagar. It is visible in Figure 10 that the system can propagate up to 1400 m in Alexandria city, which is 400 m longer than Srinagar city, and that is clear in Figure 11.

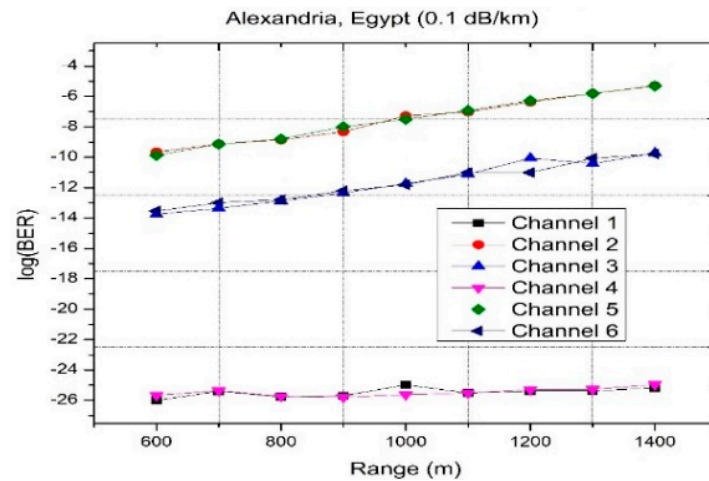


Figure 10. $\log(\text{BER})$ versus FSO link for Alexandria, Egypt.

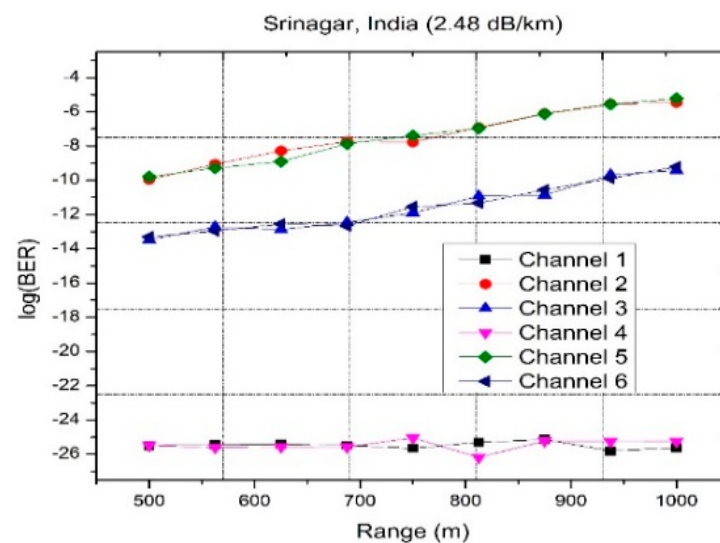


Figure 11. $\log(\text{BER})$ versus FSO link for Srinagar, India.

Table 8 summarizes the $\log(\text{BER})$ values at maximum computed FSO link for our proposed model in Alexandria city at 1400 m and in Srinagar city at 1000 m.

Variation of BER versus received optical power (ROP) under different foggy, dusty, and Alexandria and Srinagar cities' weather conditions are depicted in Figure 12. One can observe that as ROP increases, the BER improves.

Table 8. Log(BER) values at maximum computed FSO link for our proposed model in Alexandria and Srinagar cities.

Channels	OAM Beams	log(BER)	
		Alexandria City (1400 m)	Srinagar City (1000 m)
Channel #1	$LG_{0,0}$	-25.18	-25.61
Channel #2		-5.29	-5.46
Channel #3		-9.72	-9.41
Channel #4	$LG_{0,10}$	-24.96	-25.25
Channel #5		-5.31	-5.22
Channel #6		-9.78	-9.21

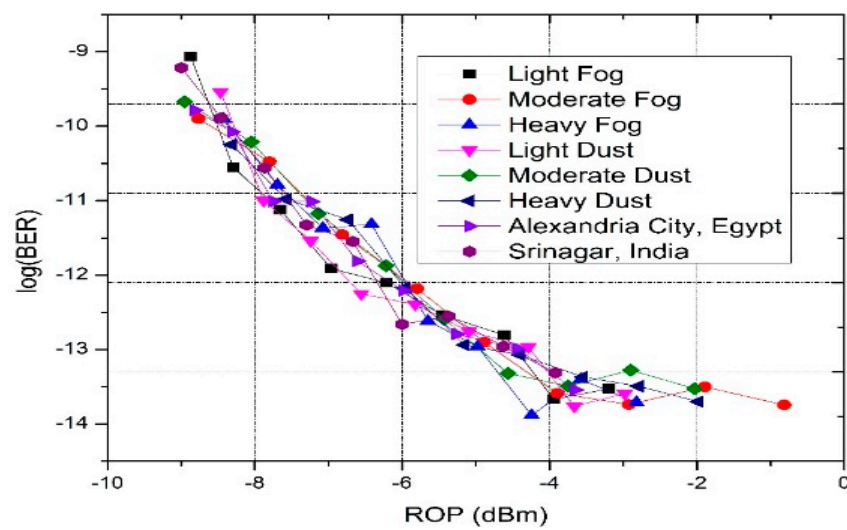


Figure 12. Log(BER) versus ROP under foggy, dusty, and Alexandria and Srinagar cities’ weather conditions.

Table 9 summarizes the comparison between different multiplexing techniques used in previous works and our present work.

Table 9. Comparison between different multiplexing techniques used in previous work and present work.

References	[27]	[52]	[53]	Present Work
Technique	NRZ-OAM-FSO	FSO	MDM-Ro-FSO	OAM-OCDMA/FRS-FSO
Laser input power	10 dBm	22 dBm	Not specified	15 dBm
Number of channels	4	1	3	6
Overall capacity	40 Gbps	2.5 Gbps	12.5 Gbps	60 Gbps
Similar weather conditions with maximum FSO link	LF: 0.48 km MF: 0.375 km HF: 0.32 km LD: 0.31 km MD: 0.13 km HD: 0.064 km	LD: 1 km MD: 0.2 km HD: <0.2 km	LF: 0.6 km MF: 0.4 km HF: 0.2 km	LF: 0.6 km MF: 0.425 km HF: 0.34 km LD: 0.315 km MD: 0.105 km HD: 0.4 km
Cities	-	-	-	Alexandria, Egypt. Srinagar, India.
Authenticated Meteorological data source	No	No	No	Yes

7. Conclusions

In this work, a novel FSO communication link is proposed by combining OAM beams with the SAC-OCDMA system. Two distinct OAM beams ($LG_{0,0}$, $LG_{0,10}$) are used, each carrying 30 Gbps of information data for three independent channels encoded with FRS code.

As weather conditions impact the performance of the FSO communication systems, in this work, we consider the effect of different fog conditions.

Additionally, as dust storms mainly occur in sand-filled areas, most researchers do not focus on studying their effect; however, in this work, we consider them and study the performance of our suggested model under their effects. Furthermore, we discuss the performance of our model using two real weather conditions of two different cities having different geographical locations: Alexandria city, which is surrounded by the sea, and Srinagar city, which contains mountains.

The performance of our proposed system is simulated and investigated in terms of BER, eye diagrams, and ROP. The obtained results show successful transmission of 60 Gbps overall capacity with acceptable BER (less than 2.7×10^{-3}) and wider eye opening that reveals successful receiving of transmitted information.

Simulated results under diverse fog conditions show that the longest FSO range obtained under LF is 600 m, which decreases to 425 m and 340 m when the fog level becomes moderate and heavy, respectively. In addition, our results show that dust storm weather conditions have a high impact and cause high attenuation, which makes the propagation link very short.

The maximum FSO links our proposed system achieves are 315 m under LD, 105 m under MD, and 40 m under HD. As Alexandria city has clear weather, it causes less attenuation and a more extended propagation range of 1400 m. While the cloudy weather of Srinagar leads to achieving an FSO link of 1000 m and its hilly area makes installing optical fiber cable difficult due to difficult terrain and mountains, we propose our FSO be implemented.

According to this study, we recommend that our model be used in the fifth-generation networks and B5G/6G, implemented in areas with different geographical locations such as deserts, seas, mountains, and smart cities.

Author Contributions: Conceptualization, S.A.A.E.-M. and M.S.; methodology, S.A.A.E.-M. and M.S.; software, S.A.A.E.-M. and M.S.; validation, S.A.A.E.-M., M.S., A.C., H.Y.A. and M.Z.; formal analysis, S.A.A.E.-M., M.S., H.Y.A. and A.N.K.; investigation, S.A.A.E.-M., M.S. and H.Y.A.; resources, S.A.A.E.-M. and M.S.; writing—original draft preparation, S.A.A.E.-M. and M.S.; writing—review and editing, A.C. and H.Y.A.; visualization, A.C. and H.Y.A.; funding acquisition, A.C. All authors have read and agreed to the published version of the manuscript.

Funding: This research received no external funding.

Data Availability Statement: Not applicable.

Conflicts of Interest: The authors declare no conflict of interest.

References

1. Dat, P.T.; Kanno, A.; Yamamoto, N.; Kawanishi, T. Seamless Convergence of Fiber and Wireless Systems for 5G and Beyond Networks. *J. Light. Technol.* **2018**, *37*, 592–605. [\[CrossRef\]](#)
2. El-Mottaleb, S.A.A.; Métwalli, A.; Chehri, A.; Ahmed, H.Y.; Zeghid, M.; Khan, A.N. New Algorithm for a Fixed Right Shift Code to Support Different Quality of Services in Smart and Sustainable Optical Networks. *Sustainability* **2022**, *14*, 10337. [\[CrossRef\]](#)
3. Lopes, C.H.d.S.; Lima, E.S.; Pereira, L.A.M.; Borges, R.M.; Ferreira, A.C.; Abreu, M.; Dias, W.D.; Spadoti, D.H.; Mendes, L.L.; Junior, A.C.S. Non-Standalone 5G NR Fiber-Wireless System Using FSO and Fiber-Optics Fronthauls. *J. Light. Technol.* **2020**, *39*, 406–417. [\[CrossRef\]](#)
4. Aveta, F.; Refai, H.H.; Lopresti, P.G. Cognitive Multi-Point Free Space Optical Communication: Real-Time Users Discovery Using Unsupervised Machine Learning. *IEEE Access* **2020**, *8*, 207575–207588. [\[CrossRef\]](#)
5. Capelle, M.; Huguet, M.-J.; Jozefowicz, N.; Olive, X. Optimizing ground station networks for free space optical communications: Maximizing the data transfer. *Networks* **2019**, *73*, 234–253. [\[CrossRef\]](#)

6. Singh, M.; Aly, M.H.; El-Mottaleb, S.A.A. Performance analysis of 6×10 Gbps PDM-SAC-OCDMA-based FSO transmission using EDW codes with SPD detection. *Optik* **2022**, *264*, 169415. [[CrossRef](#)]
7. El-Mottaleb, S.A.A.; Métwalli, A.; Hassib, M.; Alfikky, A.A.; Fayed, H.A.; Aly, M.H. SAC-OCDMA-FSO communication system under different weather conditions: Performance enhancement. *Opt. Quantum Electron.* **2021**, *53*, 616–633. [[CrossRef](#)]
8. Esmail, M.A.; Fathallah, H.; Alouini, M.S. Outdoor FSO communications under fog: Attenuation modelling and performance evaluation. *IEEE Photonics J.* **2016**, *8*, 1–22. [[CrossRef](#)]
9. Esmail, M.A.; Fathallah, H.; Alouini, M. Effect of dust storms on FSO communications links. In Proceedings of the 2016 4th International Conference on Control Engineering & Information Technology (CEIT), Hammamet, Tunisia, 16–18 December 2016; pp. 1–6.
10. Rashidi, F.; He, J.; Chen, L. Spectrum slicing WDM for FSO communication systems under the heavy rain weather. *Opt. Commun.* **2017**, *387*, 296–302. [[CrossRef](#)]
11. Jeyaseelan, J.; Kumar, S.; Caroline, B. Performance analysis of free space optical communication system employing WDM-PoISK under turbulent weather conditions. *J. Optoelectron. Adv. Mater.* **2018**, *20*, 506–514.
12. Singh, M.; Pottoo, S.N.; Malhotra, J.; Grover, A.; Aly, M.H. Millimeter-wave hybrid OFDM-MDM radio over free space optical transceiver for 5G services in desert environment. *Alex. Eng. J.* **2021**, *60*, 4275–4285. [[CrossRef](#)]
13. Chaudhary, S.; Amphawan, A.; Nisar, K. Realization of free space optics with OFDM under atmospheric turbulence. *Optik* **2014**, *125*, 5196–5198. [[CrossRef](#)]
14. Chaudhary, S.; Choudhary, S.; Tang, X.; Wei, X. Empirical evaluation of high-speed cost-effective Ro-FSO system by incorporating OCDMA-PDM scheme under the presence of fog. *J. Opt. Commun.* **2020**, *39*, 1–4. [[CrossRef](#)]
15. Krenn, M.; Handsteiner, J.; Fink, M.; Fickler, R.; Ursin, R.; Malik, M.; Zeilinger, A. Twisted light transmission over 143 km. *Proc. Natl. Acad. Sci. USA* **2016**, *113*, 13648–13653. [[CrossRef](#)]
16. Xie, G.; Li, L.; Ren, Y.; Huang, H.; Yan, Y.; Ahmed, N.; Zhao, Z.; Lavery, M.P.J.; Ashrafi, N.; Ashrafi, S.; et al. Performance metrics and design considerations for a free-space optical orbital-angular-momentum-multiplexed communication link. *Optica* **2015**, *2*, 357–365. [[CrossRef](#)]
17. Fatkhiev, D.M.; Butt, M.A.; Grakhova, E.P.; Kutluyarov, R.V.; Stepanov, I.V.; Kazanskiy, N.; Khonina, S.; Lyubopytov, V.; Sultanov, A.K. Recent Advances in Generation and Detection of Orbital Angular Momentum Optical Beams—A Review. *Sensors* **2021**, *21*, 4988. [[CrossRef](#)]
18. Dwivedi, R.; Sharma, P.; Jaiswal, V.K.; Mehrotra, R. Elliptically squeezed axicon phase for detecting topological charge of vortex beam. *Opt. Commun.* **2021**, *485*, 126710. [[CrossRef](#)]
19. Ren, Y.; Wang, Z.; Xie, G.; Li, L.; Willner, A.J.; Cao, Y.; Zhao, Z.; Yan, Y.; Ahmed, N.; Ashrafi, N.; et al. Demonstration of OAM-based MIMO FSO link using spatial diversity and MIMO equalization for turbulence mitigation. In Proceedings of the Optical Fiber Communications Conference and Exhibition (OFC), Ahaheim, CA, USA, 20–22 March 2016; pp. 1–3.
20. Zhao, L.; Liu, H.; Hao, Y.; Sun, H.; Wei, Z. Effects of atmospheric turbulence on OAM-POL-FDM hybrid multiplexing communication system. *Appl. Sci.* **2019**, *9*, 5063. [[CrossRef](#)]
21. Amhoud, E.-M.; Chafii, M.; Nimr, A.; Fettweis, G. OFDM with index modulation in orbital angular momentum multiplexed free space optical. In Proceedings of the 2021 IEEE 93rd Vehicular Technology Conference (VTC2021-Spring), Helsinki, Finland, 25–28 April 2021; pp. 1–5.
22. Ghalot, R.; Madhu, C.; Kaur, G.; Singh, P. Link Estimation of Different Indian Cities Under Fog Weather Conditions. *Wirel. Pers. Commun.* **2019**, *105*, 1215–1234. [[CrossRef](#)]
23. Prabu, K.; Charanya, S.; Jain, M.; Guha, D. BER analysis of SS-WDM based FSO system for Vellore weather conditions. *Opt. Commun.* **2017**, *403*, 73–80. [[CrossRef](#)]
24. Ali, M.A.A.; Shaker, F.K.; Kadhum, H.A. Investigation and Analysis of Data Rate for Free Space Optical Communications System Under Dust Conditions. *Wirel. Pers. Commun.* **2020**, *113*, 2327–2338. [[CrossRef](#)]
25. Ghassemlooy, Z.; Popoola, W.; Rajbhandari, S. *Optical Wireless Communication: System and Channel Modelling with Matlab*, 2nd ed.; CRC Press: Boca Raton, FL, USA, 2019.
26. Siegel, T.; Ping, S. Investigations of free space optical communications under real-world atmospheric conditions. *Wirel. Pers. Commun.* **2020**, *116*, 475–490. [[CrossRef](#)]
27. Singh, M.; Atieh, A.; Grover, A.; Barukab, O. Performance analysis of 40 Gb/s free space optics transmission based on orbital angular momentum multiplexed beams. *Alex. Eng. J.* **2022**, *61*, 5203–5212. [[CrossRef](#)]
28. Li, L.; Zhang, R.; Zhao, Z.; Xie, G.; Liao, P.; Pang, K.; Song, H.; Liu, C.; Ren, Y.; Labroille, G.; et al. High-capacity free-space optical communications between a ground transmitter and a ground receiver via a UAV using multiplexing of multiple orbital angular-momentum beams. *Sci. Rep.* **2017**, *7*, 17427. [[CrossRef](#)]
29. Ahmed, H.Y.; Nisar, K.S.; Zeghid, M.; Aljunid, S.A. Numerical Method for Constructing Fixed Right Shift (FRS) Code for SAC-OCDMA Systems. *Int. J. Adv. Comput. Sci. Appl.* **2017**, *8*, 246–252.
30. Allen, L.; Beijersbergen, M.W.; Spreeuw, R.J.C.; Woerdman, J.P.; Barnett, S.M.; Padgett, M.J. Orbital angular momentum of light and the transformation of Laguerre? Gaussian laser modes. *Opt. Angular. Momentum.* **2004**, *45*, 8185–8189.
31. Yao, A.M.; Padgett, M.J. Orbital angular momentum: Origins, behavior and applications. *Adv. Opt. Photon.* **2011**, *3*, 161–204. [[CrossRef](#)]

32. Willner, A.E.; Huang, H.; Yan, Y.; Ren, Y.; Ahmed, N.; Xie, G.; Bao, C.; Li, L.; Cao, Y.; Zhao, Z.; et al. Optical communications using orbital angular momentum beams. *Adv. Opt. Phot.* **2015**, *7*, 66–106. [[CrossRef](#)]
33. Phillips, R.L.; Andrews, L.C. Spot size and divergence for Laguerre Gaussian beams of any order. *Appl. Opt.* **1983**, *22*, 643–644. [[CrossRef](#)]
34. Willner, A.E.; Pang, K.; Song, H.; Zou, K.; Zhou, H. Orbital angular momentum of light for communications. *Appl. Phys. Rev.* **2021**, *8*, 041312. [[CrossRef](#)]
35. Xie, G.; Ren, Y.; Yan, Y.; Huang, H.; Ahmed, N.; Li, L.; Zhao, Z.; Bao, C.; Tur, M.; Ashrafi, S.; et al. Experimental demonstration of a 200-Gbit/s free-space optical link by multiplexing Laguerre–Gaussian beams with different radial indices. *Opt. Lett.* **2016**, *41*, 3447–3450. [[CrossRef](#)] [[PubMed](#)]
36. Wang, J.; Yang, J.-Y.; Fazal, I.M.; Ahmed, N.; Yan, Y.; Huang, H.; Ren, Y.; Yue, Y.; Dolinar, S.; Tur, M.; et al. Terabit free-space data transmission employing orbital angular momentum multiplexing. *Nat. Photonics* **2012**, *6*, 488–496. [[CrossRef](#)]
37. Winzer, P.J. Making spatial multiplexing a reality. *Nat. Photonics* **2014**, *8*, 345–348. [[CrossRef](#)]
38. Subekti, T.; Isnawati, A.F.; Zulherman, D. Optimization Free Space Optic (FSO) Design with Kim Model Using Space Diversity. *J. Infotel* **2019**, *11*, 93–98. [[CrossRef](#)]
39. Chaudhary, S.; Tang, X.; Wei, X. Comparison of Laguerre Gaussian and donut modes for MDM-WDM in OFDM-RoFSO transmission system. *AEU Int. J. Electron. Commun.* **2018**, *93*, 208–214. [[CrossRef](#)]
40. Singh, H.; Mittal, N.; Miglani, R.; Singh, H.; Gaba, G.S.; Hedabou, M. Design and Analysis of High-Speed Free Space Optical (FSO) Communication System for Supporting Fifth Generation (5G) Data Services in Diverse Geographical Locations of India. *IEEE Photon. J.* **2021**, *13*, 1–12. [[CrossRef](#)]
41. Mehrpoor, G.R.; Safari, M.; Schmauss, B. Free space optical communication with spatial diversity based on orbital angular momentum of light. In Proceedings of the 2015 4th International Workshop on Optical Wireless Communications (IWOW), Istanbul, Turkey, 7–8 September 2015; pp. 78–82.
42. Al-Khafaji, H.M.R.; Aljunid, S.A.; Amphawan, A.; Fadhil, H.A.; Safar, A.M. Reducing BER of spectral-amplitude coding optical code-division multiple-access systems by single photodiode detection technique. *J. Eur. Opt. Soc. Publ.* **2013**, *8*, 13022–13026. [[CrossRef](#)]
43. Singh, M.; Atieh, A.; Aly, M.H.; Abd El-Mottaleb, S.A. 120 Gbps SAC-OCDMA-OAM-based FSO transmission system: Performance evaluation under different weather conditions. *Alex. Eng. J.* **2022**, *61*, 10407–10418. [[CrossRef](#)]
44. Yousif Ahmed, H.; Zeghid, M.; A. Imtiaz, W.; Sharma, T.; Chehri, A.; Fortier, P. Two-Dimensional Permutation Vectors' (PV) Code for Optical Code Division Multiple Access Systems. *Entropy* **2020**, *22*, 576. [[CrossRef](#)]
45. El-Mottaleb, S.A.A.; Fayed, H.A.; El-Aziz, A.A.; Metawee, M.A.; Aly, M.H. Enhanced Spectral Amplitude Coding OCDMA System Utilizing a Single Photodiode Detection. *Appl. Sci.* **2018**, *8*, 1861. [[CrossRef](#)]
46. Moghaddasi, M.; Seyedzadeh, S.; Glesk, I.; Lakshminarayana, G.; Anas, S.B.A. DW-ZCC code based on SAC-OCDMA deploying multi-wavelength laser source for wireless optical networks. *Opt. Quantum Electron.* **2017**, *49*, 393–406. [[CrossRef](#)]
47. Zhang, C.; Liang, P.; Nebhen, J.; Chaudhary, S.; Sharma, A.; Malhotra, J.; Sharma, B. Performance analysis of mode division multiplexing-based free space optical systems for healthcare infrastructure's. *Opt. Quantum Electron.* **2021**, *53*, 635–648. [[CrossRef](#)]
48. Chaudhary, S.; Amphawan, A. Selective excitation of LG 00, LG 01, and LG 02 modes by a solid core PCF based mode selector in MDM-Ro-FSO transmission systems. *Laser Phys.* **2018**, *28*, 075106. [[CrossRef](#)]
49. El-Mottaleb, S.A.A.; Métwalli, A.; Chehri, A.; Ahmed, H.Y.; Zeghid, M.; Khan, A.N. A QoS Classifier Based on Machine Learning for Next-Generation Optical Communication. *Electronics* **2022**, *11*, 2619. [[CrossRef](#)]
50. Ahmed, H.Y.; Zeghid, M.; Bouallegue, B.; Chehri, A.; Abd El-Mottaleb, S.A. Reduction of Complexity Design of SAC OCDMA Systems by Utilizing Diagonal Permutation Shift (DPS) Codes with Single Photodiode (SPD) Detection Technique. *Electronics* **2022**, *11*, 1224. [[CrossRef](#)]
51. Zeghid, M.; Amaseb, K.; Ahmed, H.Y.; Khan, A.N.; Chehri, A.; Sharma, T.; Nisar, K.S. Modified Optical Burst Switching (OBS) Based Edge Node Architecture Using Real-Time Scheduling Techniques. *IEEE Access* **2021**, *9*, 167305–167321. [[CrossRef](#)]
52. Kakati, D.; Arya, S.C. Performance of grey-coded IQM-based optical modulation formats on high-speed long-haul optical communication link. *IET Commun.* **2019**, *13*, 2904–2912. [[CrossRef](#)]
53. Esmail, M.A.; Fathallah, H.; Alouini, M. An experimental study of FSO link performance in desert environment. *IEEE Commun. Lett.* **2016**, *20*, 1888–1891. [[CrossRef](#)]